# Single-Crystal EPR and X-Ray Studies of Magnetic Exchange Interactions and the Molecular Structure of Dipropylenetriamineethylenediaminecopper(II) Perchlorate, $[Cu(dpt)(en)](ClO_4)_2$

**Murugesan Velayutham,[†] Babu Varghese,[†] and Sankaran Subramanian*[,‡]**

Regional Sophisticated Instrumentation Centre, Indian Institute of Technology, Madras, Chennai-600 036, India, and Radiation Biology Branch, National Cancer Institute, National Institutes of Health, Bethesda, Maryland 20892

*Received January 22, 1998*

The monomeric copper complexes $[Cu(dpt)(en)](ClO_4)_2$ (**1**) and $[Zn/Cu(dpt)(en)](ClO_4)_2$ (**2**) (dpt = dipropylenetriamine; en = ethylenediamine) were synthesized. The complexes crystallize in space group *Pbca* with cell parameters $a$ =14.311(5) Å, $b$ = 16.638(2) Å, $c$ = 15.234(4) Å, $\alpha = \beta = \gamma = 90°$, $V$ = 3627(2) Å$^3$, and $Z$ = 8. The molecular structure of the complex tends toward trigonal bipyramidal symmetry. Angular, frequency-dependent EPR line widths and line shapes have been studied in detail to estimate the intrastack ($J$) as well as the interstack ($J'$) exchange interactions. The calculated correlation time $t_c$ for interchain spin diffusion is $1.2 \times 10^{-9}$ s using the dependence of line width at X- and Q- band frequencies. The ratio $J'/J = 6 \times 10^{-2}$ at 298 K and the line shapes indicate quasi-one-dimensional behavior. The exchange interaction pathway is most probably favored by the perchlorate anion.

## Introduction

It is essential to study the molecular properties as well as cooperative phenomena of metal complexes to understand the relationship between structure and chemical activity. By studying molecular electronic structure and bonding, it is possible to design a molecule with the desired properties. In five-coordinate copper(II) complexes, there exist two limiting forms, namely square pyramidal (sp) and trigonal bipyramidal (tbp). The stereochemistry of five-coordinate copper(II) complexes has been reviewed and discussed comprehensively by Hathaway.[1] Reinen and Atanasov have discussed the electronic states of the intermediate geometry by a vibronic coupling treatment.[2] Very few Cu(II) complexes with regular TBP geometry are known.[3,4] The two forms can be easily recognized from the ESR spectra, since $g_\perp > g_\parallel \approx 2.00$ and $|A_\parallel| \approx |A_\perp| \approx 60-100$ G for trigonal and $g_\perp < g_\parallel$ and $|A_\perp| \ll |A_\parallel| \approx 120-150$ G for square pyramidal complexes.[5]

In the neat systems, the molecules generally undergo magnetic exchange interactions. The exchange couplings, depending on the three-dimensional arrangement of the molecules in the lattice, may be of different dimensionalities. Low-dimensional magnetic materials have highly anisotropic magnetic, electrical, and optical properties. Much effort has been devoted to understanding the orbital mechanisms of exchange interactions, in order to design polymetallic complexes with predictable magnetic properties.[6] An important quantity in the understanding of spin dynamics is the degree of dimensionality, i.e., the ratio of the interchain to intrachain exchange coupling, $J'/J$.[7] In most of the systems, the intrachain exchange coupling is greater than the interchain interactions. Systems with strong exchange coupling will give "exchange narrowed" lines in EPR spectra. Studies of temperature- and frequency-dependent angular variations of $g$ values and line shape analysis will yield information regarding local magnetic interactions.[8] Kuppusamy and Manoharan have estimated the intersite exchange coupling $J'$ in $[NMe_4]_2[Cu(mnt)_2]$ (mnt = maleonitriledithiolato) using frequency-dependent line width and temperature variation studies.[9]

There are different pathways for exchange interactions between molecules. Even when there are no bridging ligands between molecules, there can be exchange interactions taking place via the counterions. The perchlorate counteranion in $[Cu_2(Me_5dien)_2(C_2O_4)](ClO_4)_2$ has been inferred to be involved in exchange interactions, and hydrogen bonding acting as a pathway for exchange interactions has been found in $(dabcoH_2)_2Cl_3[CuCl_3(H_2O)_2]\cdot H_2O$.[4,10,11] In pure systems, it is difficult to study the molecular properties due to exchange coupling. Hence, the complex is diluted in a diamagnetic isomorphous lattice and the molecular properties are studied.

Ponticelli concluded that the structure of the title complex is square pyramidal using IR and optical absorption techniques.[12]

[†] Indian Institute of Technology.
[‡] National Cancer Institute.

(1) Hathaway, B. J. *Comprehensive Coordination Chemistry*; Pergamon: Oxford, U.K., 1987; p 533.
(2) Reinen, D.; Atanasov, M. *Chem. Phys.* **1989**, *136*, 27.
(3) Duggan, M.; Ray, N.; Hathaway, B. *J. Chem. Soc., Dalton Trans.* **1980**, 1342.
(4) Wei, M.; Willet, R. D. *Inorg. Chem.* **1996**, *35*, 6381.
(5) Bencini, A.; Bertini, I.; Gatteschi, D.; Scozzafava, A. *Inorg. Chem.* **1978**, *17*, 3194.
(6) Kahn, O. *Angew. Chem., Int. Ed. Engl.* **1985**, *24*, 834.
(7) Richards, P. M. *Low Dimensional Cooperative Phenomena*; Plenum Press: New York, 1975.
(8) Soos, Z. G.; Huang, T. Z.; Valentine, J.; Hughes R. C. *Phys. Rev. B* **1973**, *8*, 993.
(9) Kuppusamy, P.; Manoharan P. T. *Inorg. Chem.* **1985**, *24*, 3053.
(10) Felthouse, T. R.; Laskowski, E. J.; Hendrickson, D. N. *Inorg. Chem.* **1977**, *16*, 1077.
(11) Balagopalakrishna, C.; Rajasekharan, M. V. *Phys. Rev. B* **1990**, *42*, 7794.
(12) Ponticelli, G. *Inorg. Chim. Acta* **1971**, *5*, 461.

10.1021/ic980071n CCC: $15.00 
Published on Web 10/20/1998

**Table 1.** Crystal Data and Structure Refinement Details for $[Cu(dpt)(en)](ClO_4)_2$

| | |
|---|---|
| empirical formula | $C_8H_{25}Cl_2CuN_5O_8$ |
| formula weight | 453.77 |
| temp | 293(2) K |
| wavelength | 1.5418 Å |
| space group | *Pbca* (No. 61) |
| unit cell dimens | $a = 14.311(5)$ Å, $b = 16.638(2)$ Å, $c = 15.234(4)$ Å, $\alpha = 90°$, $\beta = 90°$, $\gamma = 90°$ |
| volume | 3627(2) Å$^3$ |
| $Z$ | 8 |
| density (calcd) | 1.662 g cm$^{-3}$ |
| abs coeff | 48.48 cm$^{-1}$ |
| $R(F)^a$ | 0.0591 |
| $R_w(F^2)^b$ | 0.1838 |

$^a$ $R(F) = \sum||F_o| - |F_c||/\sum|F_o|$. $^b$ $R_w(F^2) = \{\sum[w(F_o^2 - F_c^2)]^2/\sum(wF_o^2)^2\}^{1/2}$. $w = 1/\{[\sigma(F_o^2)]^2 + (0.1042P)^2 + (8.2685P)\}$ where $P = [\mathrm{Max}(F_o^2, 0) + 2F_c^2]/3$. $S = \{\sum[w(F_o^2 - F_c^2)]^2/(n - p)\}^{1/2}$.

The important structural features, angular variation of $g$ values as well as line widths, and the exchange interaction of the title complex will be discussed on the basis of the electronic, IR, single-crystal XRD, and X- and Q-band EPR results obtained in the solid and solution states.

## Experimental Section

*Caution*! Perchlorate complexes of metal ions are potentially explosive. Only small amounts of material should be prepared, and they should be handled with great care.

**Preparation of $[Cu(dpt)(en)](ClO_4)_2$.** Equimolar amounts of dipropylenetriamine (dpt) and ethylenediamine (en) (5 mmol each) in a 2:1 water−alcohol mixture were added to a warm aqueous solution of copper acetate (5 mmol). To this mixture was added dropwise a solution of sodium perchlorate in water until precipitation was complete. The resulting solid was filtered off, washed with a water−alcohol mixture, and dissolved in hot water. Prismatic crystals formed after a few days. The isomorphous zinc complex was also synthesized using an identical procedure by replacing copper(II) acetate with zinc(II) acetate.

**Physical Measurements.** Solution, polycrystalline, and single-crystal EPR spectra (X- and Q- bands) at 300 and 77 K were recorded on a Varian E112 EPR spectrometer. IR spectra were recorded on a Bruker IFS 66v FT-IR spectrometer in KBr matrixes, and UV/vis spectra were recorded on a Shimadzu UV-3100 spectrometer.

**X-ray Crystallography.** A single crystal of approximate dimensions $0.3 \times 0.2 \times 0.1$ mm was mounted on the goniometer of an Enraf Nonius CAD-4 single-crystal X-ray diffractometer. Graphite-monochromated Cu K$\alpha$ radiation ($\lambda = 1.5418$ Å) was used for the diffraction studies. The unit cell parameters were obtained from the method of shortest vectors followed by a least-squares calculation using 25 centered reflections. The intensity data were collected in the range $2° < \theta < 70°$ using a moving-crystal, moving-detector ($\omega-2\theta$) scan technique. A total of 3441 unique reflections were measured, of which 3121 reflections having intensity $I \geq 2\sigma(I)$ were considered and used in the structure determination. The data were corrected for Lorentz and polarization effects. Intensities of two strong reflections were monitored once in every hour of X-ray exposure time to check for possible deterioration of the crystal and instrument instability during data collection. Crystal orientation checks were performed every 400 reflections. The absorption correction was effected using $\psi$ scan data.

The structure was solved by direct methods using the SHELX-86 computer program and refined by the full-matrix least-squares method using the SHELXL-93 computer program. Although, all the hydrogen atoms in the molecule could be located from a difference electron density map, they were placed at the respective calculated positions and a Riding model refinement was performed. The final residual factors were $R(F) = 0.0591$ and $R_w(F^2) = 0.1838$. The quantity minimized in the least-squares refinement was $\sum w(F_0^2 - F_c^2)^2$. All pertinent crystallographic data are given in Table 1. An examination of the crystals of the Zn complex showed that it is isomorphous with the Cu(II) complex.

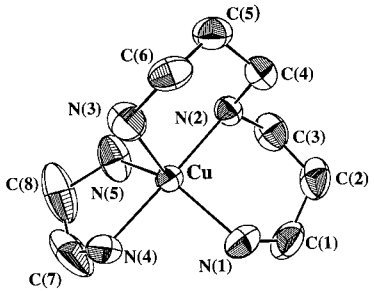


**Figure 1.** ORTEP representation of the molecule depicting 50% probability ellipsoids and the numbering scheme for $[Cu(dpt)(en)]^{2+}$.

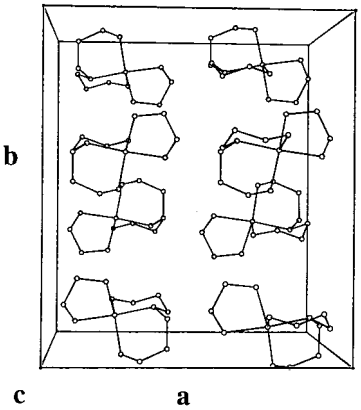


**Figure 2.** Projection of the crystal structure of $[Cu(dpt)(en)]^{2+}$ along the $c$ axis. (For clarity, the perchlorate ions have been omitted.)

## Results and Discussions

**Description of the Structure.** The complexes $[Cu(dpt)(en)](ClO_4)_2$ (**1**) and $[Zn/Cu(dpt)(en)](ClO_4)_2$ (**2**) are isomorphous. The molecules crystallize in space group *Pbca* with 8 molecules per unit cell. The lattice consists of $[M(dpt)(en)]^{2+}$ (M = Cu, Zn) cations and $ClO_4^-$ anions. The cationic structure of the complex is given in Figure 1. Figure 2 presents the packing diagram of the complex projected along the $c$ axis.

The structure of the cation involves a five-coordinated $CuN_5$ chromophore with no evidence for even a weak coordination of the $ClO_4^-$ anions. In short, the stereochemistry of the coordination polyhedron can be viewed as close to a compressed trigonal bipyramid (TBP) similar to those reported for several cations.[13] Such a stereochemistry for five-coordinated copper(II) systems is slightly stabilized if significant steric hindrance is present.[2] Selected bond lengths and bond angles for complex **1** are given in Table 2. The Cu−N bond distances are in the range 2.018−2.129 Å found in similar compounds.[14] Here all the Cu−N bond lengths are different. Therefore, the molecular symmetry is $C_s$. The single secondary nitrogen atom, N(2), of the dpt ligand occupies an axial coordination site, whereas the two primary nitrogen atoms, N(1) and N(3), occupy equatorial sites. The remaining two Cu(II) TBP coordination sites are occupied by two primary nitrogen atoms, N(4) and N(5), from the en ligand. The Cu−N(2) bond makes small angle of ~12° with the crystallographic $a$ axis. The two six-membered rings and a five-membered ring formed by dpt and en have strain-

(13) Garcia-Lozano, J.; Server-Carrio, J.; Escriva, E.; Folgado, J.; Molla, C.; Lezama, L. *Polyhedron* **1997**, *16*, 939.
(14) Ullah, M. R.; Bhattacharya, P. K.; Venkatasubramanian, K. *Polyhedron* **1996**, *15*, 4025.

**Table 2.** Selected Bond Lengths (Å) and Angles (deg) for $[Cu(dpt)(en)](ClO_4)_2$[a]

| | | | |
|---|---|---|---|
| Cu−N(1) | 2.036(5) | Cl(1)−O(3) | 1.318(8) |
| Cu−N(2) | 2.018(4) | Cl(1)−O(4) | 1.396(8) |
| Cu−N(3) | 2.110(5) | Cl(2)−O(5) | 1.445(8) |
| Cu−N(4) | 2.038(6) | Cl(2)−O(6) | 1.392(7) |
| Cu−N(5) | 2.129(6) | Cl(2)−O(7) | 1.406(8) |
| Cl(1)−O(1) | 1.293(9) | Cl(2)−O(8) | 1.399(7) |
| Cl(1)−O(2) | 1.414(7) | | |
| N(2)−Cu−N(1) | 91.2(2) | N(2)−Cu−N(4) | 174.0(3) |
| N(1)−Cu−N(4) | 91.2(3) | N(2)−Cu−N(3) | 92.1(2) |
| N(1)−Cu−N(3) | 125.7(3) | N(4)−Cu−N(3) | 91.0(2) |
| N(2)−Cu−N(5) | 91.0(2) | N(1)−Cu−N(5) | 130.9(3) |
| N(4)−Cu−N(5) | 83.2(3) | N(3)−Cu−N(5) | 103.3(3) |

[a] Symmetry transformations used to generate equivalent atoms: $-x, -y, -z$; $^1/_2 - x, -y, ^1/_2 + z$; $^1/_2 + x, y, ^1/_2 - z$; $-x, ^1/_2 + y, ^1/_2 - z$; $x, ^1/_2 - y, ^1/_2 + z$; $^1/_2 + x, ^1/_2 - y, -z$; $^1/_2 - x, ^1/_2 + y, z$.

free chair and envelope conformations, respectively. The coordination geometry around Cu(II) in $[Cu(det)(en)](ClO_4)_2$ (det = diethylenetriamine) is square pyramidal.[14] In complex **1**, replacing the chelating en ligand by thiocyanate ligands with the nitrogen end coordinating leads to a square pyramidal geometry.[15] The square pyramidal geometry of the thiocyanate complex is due to the release of the strain.

The distorted trigonal bipyramidal geometry of complex **1** is due to the steric enhancement of the dpt and en ligands in the basal plane. The in-plane bond angles are far from the value of 120° expected for a regular TBP stereochemistry. The equatorial coordination was found to be planar (with the sum of the three angles ≈360°). The calculated $\tau$ [$(\beta - \alpha)/60$] value from the bond angles of 0.72 (1 for perfect trigonal bipyramidal geometry) clearly indicates the predominance of the TBP form but with a significant degree of distortion toward the SP topology. The shortest Cu- - -Cu distance is 7.86 Å. The canting angle 2α, which is the angle between the two normals to the equatorial planes of the two differently oriented molecules, is 24°.

The two perchlorate anions are not coordinated to the cations. They separate the cations such that the shortest intermolecular Cu- - -Cu distance is greater than 7 Å. There is some disorder or libration of the perchlorate anions, which is reflected in some rather short apparent Cl−O distances. The bond angles vary from 103 to 115°.

**Vibrational and Electronic Spectra.** Ponticelli concluded that the structure of complex **1** was square pyramidal with the help of IR and electronic spectral studies.[12] A powder optical reflectance spectrum of complex **1** showed a peak at $15.4 \times 10^3$ $cm^{-1}$ and a shoulder at $11.4 \times 10^3$ $cm^{-1}$ and a spectrum in methanol solution showed a peak at $14.8 \times 10^3$ $cm^{-1}$ and a shoulder at $12.5 \times 10^3$ $cm^{-1}$.

Our IR spectral data agree fairly well with the already published results. The bands in the 1080−1150 $cm^{-1}$ region belong to the asymmetric stretching vibration of the uncoordinated tetrahedral perchlorate anion, the peaks in the 3135−3475 $cm^{-1}$ region correspond to stretching vibrations $\nu(NH_2)$ and $\nu$(NH), and the peak at 1602 $cm^{-1}$ is assigned to $\delta(NH_2)$.

Solution optical spectra in different solvents were recorded at room temperature, and the parameters are given in the Table 3. In all the spectra, the high-energy peak is more intense than the lower energy peak. In methanol, DMF, and DMSO, the spectra are similar and the peaks occur at similar energy values. The nature of the peak corresponds to a change in coordination from five to six. In water, the peaks show a blue shift, which may be due to a possible change in the molecular symmetry. In a mixture of water and pyridine, the shoulder completely vanishes and the high-energy peak is blue-shifted. This disappearance of the low-energy peak shows that the geometry changes from five- to six-coordination with octahedral symmetry. The occurrence of a shoulder around $11-12 \times 10^3$ $cm^{-1}$, however, shows that the molecular structure is tending toward $O_h$ symmetry. Among all the solvents studied, pyridine has the greatest effect on the molecular structure and probably acts as the sixth ligand.

**Table 3.** Parameters of Electronic Spectra for $[Cu(dpt)(en)](ClO_4)_2$

| | $10^3$ $cm^{-1}$ | |
|---|---|---|
| solvent | peak I | peak II (shoulder) |
| water | 16.22 | 11.69 |
| methanol | 15.47 | 12.38 |
| DMF | 15.47 | 12.38 |
| DMSO | 15.19 | 12.34 |
| water−pyridine | 17.05 | |

**Table 4.** EPR Parameters for $[Cu(dpt)(en)](ClO_4)_2$ at 300 K

| solvent | $g_{iso}$ | $A_{iso}$, G |
|---|---|---|
| water | 2.1222 | 81.7 |
| water−pyridine | 2.1257 | 78.3 |
| methanol | 2.1310 | 65.0 |
| DMSO | 2.1424 | 68.3 |
| DMF | 2.1308 | 65.8 |

**Electron Paramagnetic Resonance Spectroscopy. (i) Solution EPR.** All the EPR parameters for the solution spectra of **1** recorded at 300 and 77 K are given in Tables 4 and 5. The solution EPR spectra at 300 K are given in Figure 3. In water and in a water−pyridine mixture, the $A_{iso}$ values are close to each other. All four of the lines corresponding to hyperfine coupling from Cu ($I = ^3/_2$) are well resolved due to a complete averaging effect. In all other solvents, the $A_{iso}$ value is less than that in water and the low-field peaks are broadened. The broadening of the low-field lines is due to incomplete averaging of the transitions corresponding to the anisotropic **g** and **A** tensors of the molecule. The change in the $A_{iso}$ value for different solvents shows that the unpaired electron is delocalized to the solvent molecule although there is no resolved superhyperfine structure from the additional ligands of the solvent. At room temperature, the molecular structures in methanol, DMF, and DMSO are likely to be identical.

At 77 K, water is not a good solvent matrix for isolating the paramagnetic molecules. All the molecules are aggregated and give a spectrum similar to that of the powder. In a water−pyridine mixture, the frozen-solution spectrum (Figure 4a) gives rhombic $g$ values. The low-field region shows the quartet hyperfine structure from Cu ($I = ^3/_2$), and in the high-field region couplings due to either Cu ($A_\perp$) and/or ligand nitrogens ($I = 1$) are seen.

In methanol, DMSO, and DMF, all the spectra are identical with axially symmetric $g$ values. The parallel region is resolved with hyperfine splitting from the copper. The frozen-glass spectrum in methanol is given in Figure 4b. The $A_\parallel$ value of ∼170 G is much larger than the molecular value of 126 G for the complex diluted in the isomorphous zinc lattice. It is well-known that a $d_{x^2-y^2}$ ground state for Cu(II) octahedral complexes with tetragonal elongation leads to a large parallel Cu hyperfine coupling whereas a $d_{z^2}$ ground state that can be found in a trigonal bipyramidal or compressed octahedral environment will give a much reduced parallel Cu hyperfine coupling. This is because, in the former case, the dipolar and isotropic hyperfine

(15) Cannas, M.; Carta, G.; Marongiu, G. *J. Chem. Soc., Dalton Trans.* **1974**, 556.

**Table 5.** EPR Parameters for $[Cu(dpt)(en)](ClO_4)_2$ at 77 K

| solvent | $g_1$ | $g_2$ | $g_3$ | $A_1$, G | $A_2$, G | $A_3$, G |
|---|---|---|---|---|---|---|
| water | 2.1554 | | 2.0374 | | | |
| water−pyridine | 2.2258 | 2.0595 | 2.0130 | 183.3 | 17.0 | 16.7 |
| methanol | 2.2227 | 2.0322 | 2.0322 | 160.0 | 36.6 | 36.6 |
| DMSO | 2.2078 | 2.0277 | 2.0277 | 162.5 | 35.0 | 35.0 |
| DMF | 2.2116 | 2.0277 | 2.0277 | 170.0 | 35.0 | 35.0 |

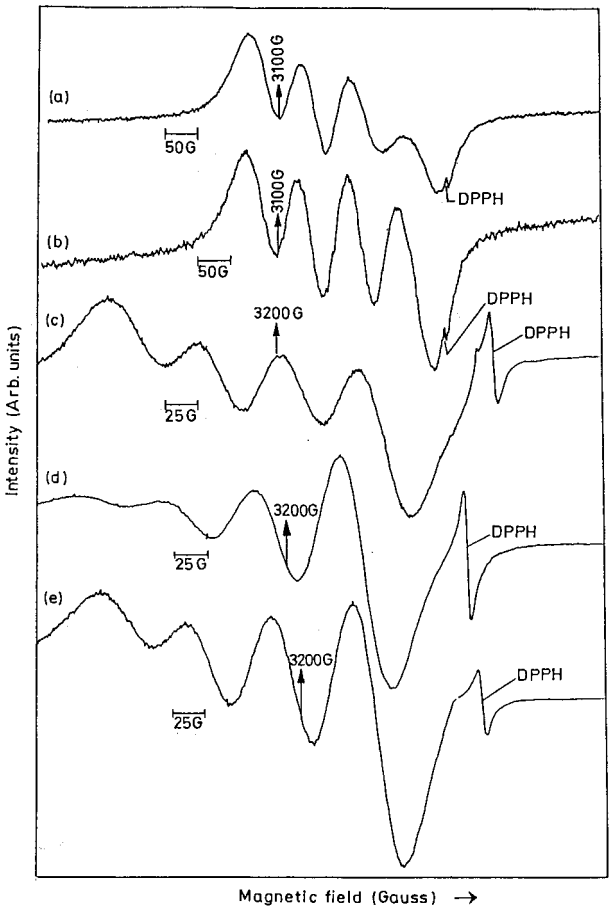


**Figure 3.** Solution X-band EPR spectra of $[Cu(dpt)(en)](ClO_4)_2$: (a) in water; (b) in a water−pyridine mixture; (c) in methanol; (d) in DMSO; (e) in DMF.

couplings are of the same sign (negative) whereas, in the latter, the dipolar coupling is positive. Therefore there seems to be a change in the ground state of the Cu(II) complex in frozen solution with the unpaired electron occupying formally a $d_{x^2-y^2}$ orbital.

**(ii) Polycrystalline EPR.** The X- and Q-band polycrystalline EPR spectra were recorded for complexes **1** and **2** at 77 and 300 K. Sastry et al. and Madhu et al. studied the polycrystalline EPR spectra for complexes of the cation $[Cu(dpt)(en)]^{2+}$ with different anions such as $Cl^-$, $Br^-$, $I^-$, and $BPh_4^-$.[16,17] They concluded that the structure of the cation for the first three complexes was trigonal bipyramidal (TBP) and the last one was square pyramidal (SP). Here, in complexes **1** and **2**, the cationic structure tends toward TBP.

For complex **2**, a 300 K EPR spectrum recorded at X-band gives a poorly resolved pattern (Figure 5a). For the same complex, a Q-band spectrum gives the molecular $g_1^{mol}$, $g_2^{mol}$, and $g_3^{mol}$ values as 2.1949, 2.1236, and 2.0244, respectively

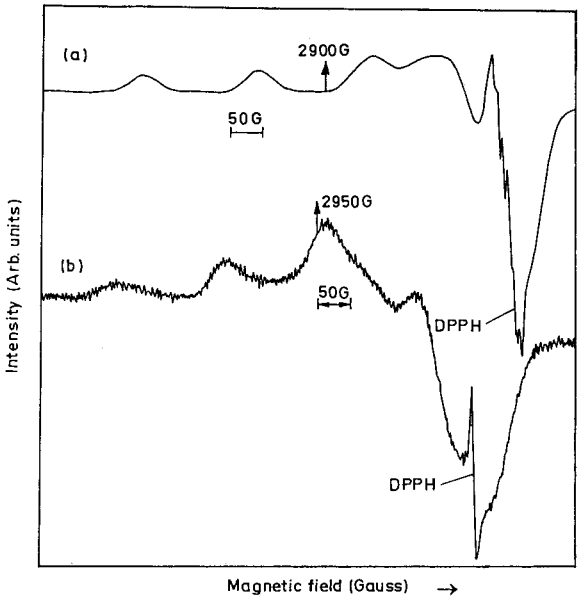


**Figure 4.** X-band frozen-solution EPR spectra of $[Cu(dpt)(en)](ClO_4)_2$ at 77 K: (a) in a water−pyridine mixture; (b) in methanol.

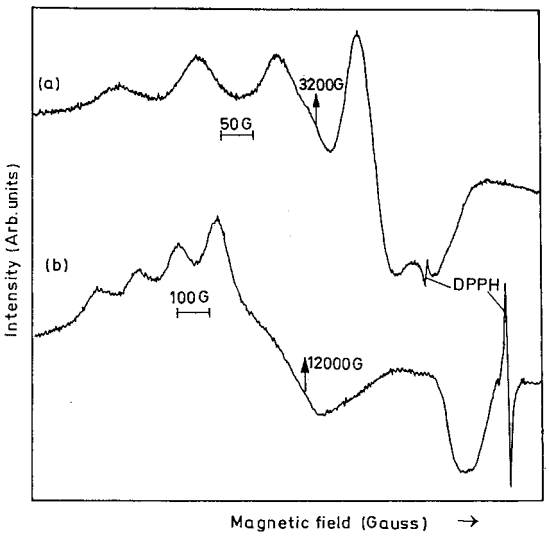


**Figure 5.** Polycrystalline EPR spectra of $[Cu(dpt)(en)](ClO_4)_2$/$[Zn(dept)(en)](ClO_4)_2$ at room temperature: (a) X-band; (b) Q-band.

(Figure 5b). The $g_1^{mol}$ and $g_2^{mol}$ values are different because the bond lengths in the equatorial planes are not equal. In the low-field region, the hyperfine splittings are well resolved and the magnitude is 126 G. The minimum $g^{mol}$ value and the maximum hyperfine value are in the limit expected for $D_{3h}$ symmetry, and hence the formal ground state is $d_{z^2}$.[18]

The X-band spectrum of **1** recorded at 300 K gives an axially symmetric pattern with the low-field region broadened due to the closeness of the two $g$ values. The hyperfine splitting from the copper nucleus and superhyperfine splitting from the

(16) Sastry, B. A.; Madhu, B.; Ponticelli, G.; Massacesi, M. *J. Phys. Soc. Jpn.* **1988**, *57*, 1140.
(17) Madhu, B.; Sastry, B. A.; Ponticelli, G.; Puggioni, G. *J. Phys. Soc. Jpn.* **1990**, *59*, 3487.
(18) Bencini, A.; Bertini, I.; Gatteschi, D.; Scozzafava, A. *Inorg. Chem.* **1978**, *17*, 7, 3194.

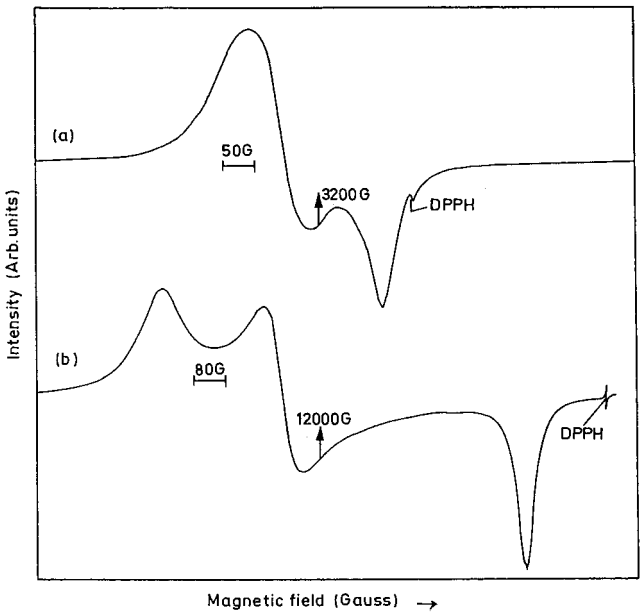


**Figure 6.** Polycrystalline EPR spectra of $[Cu(dpt)(en)](ClO_4)_2$ at room temperature: (a) X-band; (b) Q-band.

nitrogen ligands are also not resolved (Figure 6a). The EPR spectrum recorded at 77 K shows that there is no change in the nature of the peaks. The high-field $g$ value is close to the free-spin value, confirming the $d_{z^2}$ ground state. In the Q-band spectrum also, the nuclear and superhyperfine structures are not resolved (Figure 6b). The absence of hyperfine and superhyperfine structure is due to the dipolar and exchange interactions of the molecules with the nearest molecules in the neat system. The hyperfine splittings are broadened into a single line since the nearest Cu- - -Cu distances are greater than 7 Å and the contribution due to the dipolar coupling will be very low.

If it is merely due to dipolar broadening from the nearest neighbors, then the line width should be around ~360 G; but here it is only 160 G. Therefore the reduction in the line width is due to exchange narrowing. The approximate range of $J$ is

$$A(\text{hyperfine}), D(\text{dipolar}) < J < g\beta B_0(\text{X- and Q-bands})$$

The $g$ values obtained from the Q-band spectrum subject to exchange coupling effects are $g_1^{ex} = 2.1970$, $g_2^{ex} = 2.1395$, and $g_3^{ex} = 2.0356$. From the exchange-influenced $g$ values, $2\alpha$ can be calculated from[19]

$$\cos 2\alpha = (g_1^{ex} - g_2^{ex})/(g_1^{ex} + g_2^{ex} - 2g_3^{ex}) \qquad (1)$$

The calculated value is 77.48°. From this, the molecular $g$ values are calculated from

$$g_1^{ex} = g_1(\cos^2 \alpha) + g_2(\sin^2 \alpha)$$

$$g_2^{ex} = g_2(\cos^2 \alpha) + g_1(\sin^2 \alpha)$$

$$g_3^{ex} = g_3 \qquad (2)$$

which are $g_1$, $g_2$, and $g_3$. Using $2\alpha$ derived from the XRD data and the experimentally obtained exchange-averaged $g$ values, we can obtain another set of molecular $g$ values. The latter values derived are close to the actual experimental molecular $g$ values derived from the diamagnetically diluted system **2**. The ratio $[(g_1 - g_2)/(g_2 - g_3)]$, is 1.8 which shows that the symmetry is TBP.

**(iii) Single-Crystal EPR.** Single-crystal EPR measurements were carried out for complex **1**. The crystallographic *a*, *b*, and *c* axes were chosen for the single-crystal EPR measurements. With respect to these three axes, the magnetic field scaned the $g$ values in the three mutually perpendicular planes at regular intervals of rotation. Room-temperature angular variation of the $g$ values in all three planes was explored at both X- and Q-bands. The external morphology of the crystal selected for the angular variation was cubic, and the three edges corresponded to the *a*, *b*, and *c* directions. Spectra were measured with the magnetic field scanning the three planes *ab*, *bc*, and *ac*. A single line was observed in all orientations, in all three planes. Hyperfine splitting and zero-field splitting were not observed in the spectra at any crystal orientation. Generally, the hyperfine structure was not resolved in the EPR spectra of magnetically concentrated copper(II) compounds. From the crystal structure, we expected two magnetically distinct sites in the *ab* and *ac* planes and only one site in the *bc* plane.

The EPR spectrum of a system with an orthorhombic **g** tensor is described by the angle-dependent $g$ value

$$g(\theta) = (g_1^2 \cos^2 \theta_1 + g_2^2 \cos^2 \theta_2 + g_3^2 \cos^2 \theta_3)^{1/2} \qquad (3)$$

The plots of the angular variation of the $g$ values in all three planes at X- and Q-band frequencies are given in the Figure 7. The $g$ value variations at both frequencies agree very well. There is an excellent agreement between the theoretically calculated $g$ values from eq 3 and the experimental $g$ values. The method of Schonland was used to determine the $g^2$ matrix elements.[20] From the Q-band data, a simple diagonalization procedure yielded the principal values $g_1^{ex} = 2.1843$, $g_2^{ex} = 2.1345$, and $g_3^{ex} = 2.0305$. The principal $g$ values are consistent with the powder $g$ values. The direction cosines of the principal values coincide with the *a*, *b*, and *c* axes. $g_3^{ex}$ is along the crystallographic *a* axis, $g_2^{ex}$ is along the *b* axis, and $g_1^{ex}$ is along *c* axis; the $g^{ex}$ values are the site-independent exchange-averaged values.

There are two different magnetically inequivalent sites in the unit cell, as per the XRD data. The two sites are due to the differences in the angle made by the Cu−N bonds with respect to the crystal axes governed by the space group (*Pbca*). To rationalize the presence of only a single magnetically distinct site in the unit cell (the molecular disposition in the lattice leads to two distinct sites in the *ab* and the *ac* planes), we now examine the theoretically expected angular variation of the $g$ values in the absence of "exchange" using the molecular $g$ values derived from the diluted system. We consider the molecular $g_3^{mol}$ and $g_2^{mol}$ directions to be along the Cu−N(2) and Cu−N(1) bonds, respectively, and that of $g_1^{mol}$ to be perpendicular to the above two directions. The orientations of the $g^{mol}$ axes within the molecular framework are shown in Figure 8. Angular variation of the $g$ values is calculated using the principal $g$ values derived from the diluted system and the single-crystal XRD data. In the plane that is perpendicular to the Cu−N(2) axis, the two spatially distinct sites per unit cell are magnetically equivalent and have identical $g$ values in all directions. In the other two planes, there are two different resonances in general orientations corresponding to two magnetically inequivalent sites. The average value of the two

(19) Henke, W.; Kremer, S.; Reinen, D. *Inorg. Chem.* **1983**, *22*, 2858.

(20) Schonland, D. S. *Proc. Phys. Soc.* **1959**, *73*, 788.

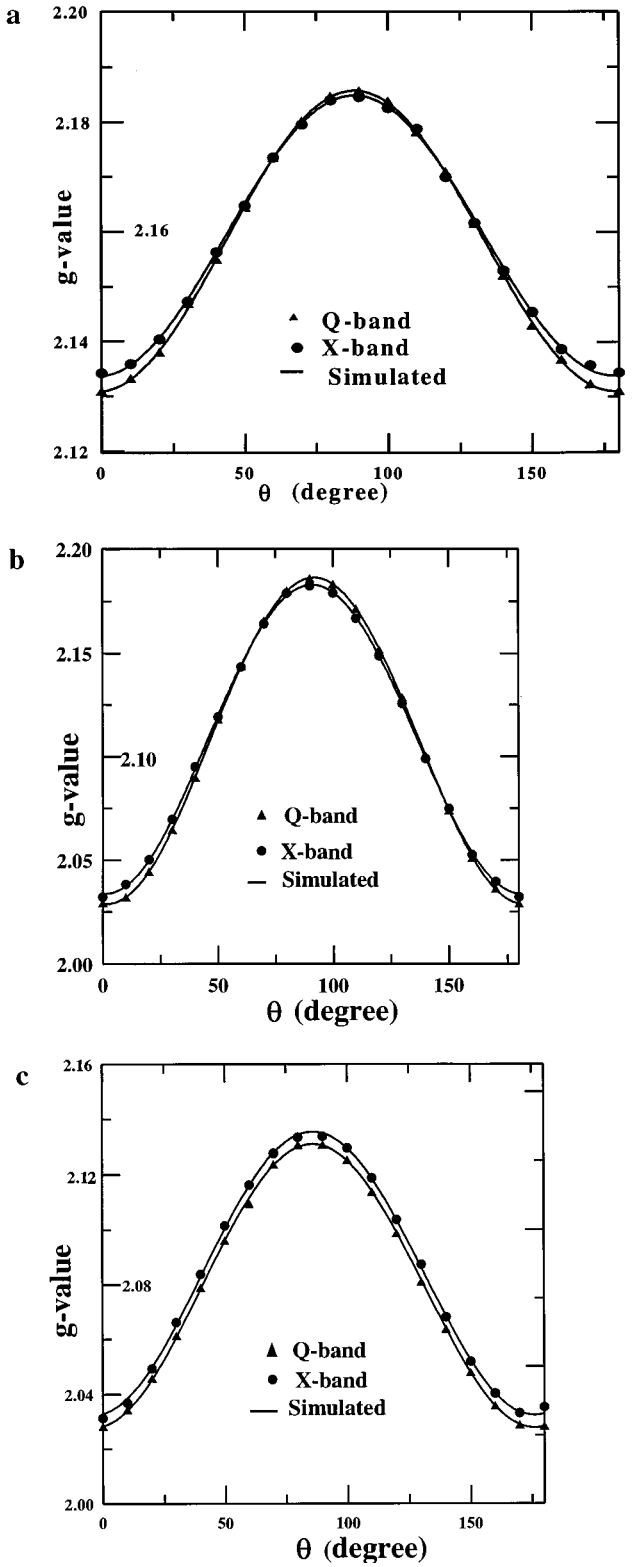


**Figure 7.** Experimental and calculated angular variations of *g* values in the (a) *bc*, (b) *ac* and (c) *ab* planes for $[Cu(dpt)(en)](ClO_4)_2$.

molecular *g* values in these two planes agrees reasonably well with the experimental "exchange-averaged" *g* values.

Using the atomic coordinates from XRD data and projections of the molecule in the planes, the direction cosines of the exchange-averaged *g* values can be rationalized. The Cu−N(2) bond makes a small angle with the *a* axis in the unit cell. The $g_3^{ex}$ direction is very close to the pseudo-$C_3$ axis of the TBP symmetry. The $g_2^{ex}$ direction is closer to the Cu−N(1) bond,

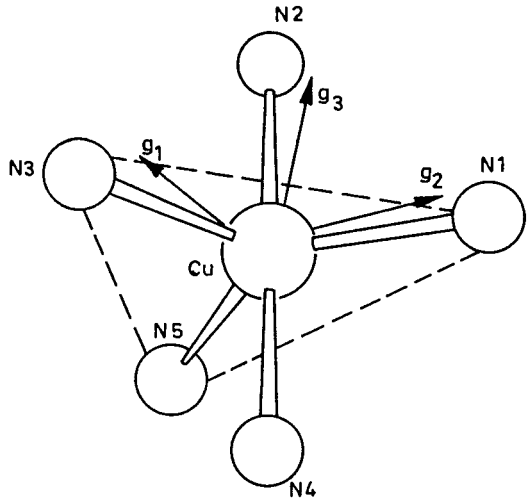


**Figure 8.** Orientation of **g** tensor principal axes with respect to the molecular frame of $[Cu(dpt)(en)](ClO_4)_2$.

which is the shortest bond in the equatorial plane, and the $g_1^{ex}$ direction is mutually orthogonal to the above two directions.

**(a) Line Widths.** In the EPR spectra of magnetically concentrated systems, generally the observed line width is the resultant of two opposing factors—the dipolar interaction, which broadens the line, and the exchange interaction which narrows the line. In three-dimensional systems, quite often, the exchange effects dominate and the lines are narrowed. In one-dimensional systems, the exchange is much less effective and the line widths are intermediate between the exchange-narrowed and dipolar-broadened limits.[21] The line widths at X- and Q-band frequencies are compared for differences. When no significant difference is observed between X- and Q-band measurements, it can be inferred that the exchange interaction, *J*, is far from X- and Q-band frequencies, i.e.

$$B_{ex} \gg B_Q > B_X \quad \text{or} \quad B_{ex} \ll B_X < B_Q$$

In the former case, both secular and nonsecular components of the hyperfine and dipolar fields will be contributing fully to the observed line width, while, in the latter case, only secular components will be effective in broadening the observed line. In the intermediate cases, with

$$B_X < B_{ex} < B_Q$$

one would observe frequency-dependent line widths as the nonsecular contributions to the Q-band line widths are only partial. In the present case, the system is not in the intermediate region.

The line width variation in our system in the three planes at X-band does not follow the $|3\cos^2\theta - 1|^{4/3}$ dependence. At Q-band, in planes *ab* and *bc*, the line width variation follows the $|3\cos^2\theta - 1|^{4/3}$ dependence. The angular variations of the line widths at X- and Q-band for the *bc*, *ac*, and *ab* planes are given in the Figure 9. The line widths at Q-band are always larger than those at X-band in all orientations. This is due to the fact that $\Delta g$ expressed in field units is 4 times larger in Q-band than in X-band, and there would be a tendency for the two sites to become resolved. However, even in Q-band, there is only one peak in each orientation. This is because the exchange coupling is greater than the $\Delta g$ (between the two

(21) Gatteschi, D.; Guillou, O.; Zanchini, C.; Sessoli, R.; Kahn, O.; Verdaguer, M.; Pei, Y. *Inorg. Chem.* **1989**, *28*, 287.

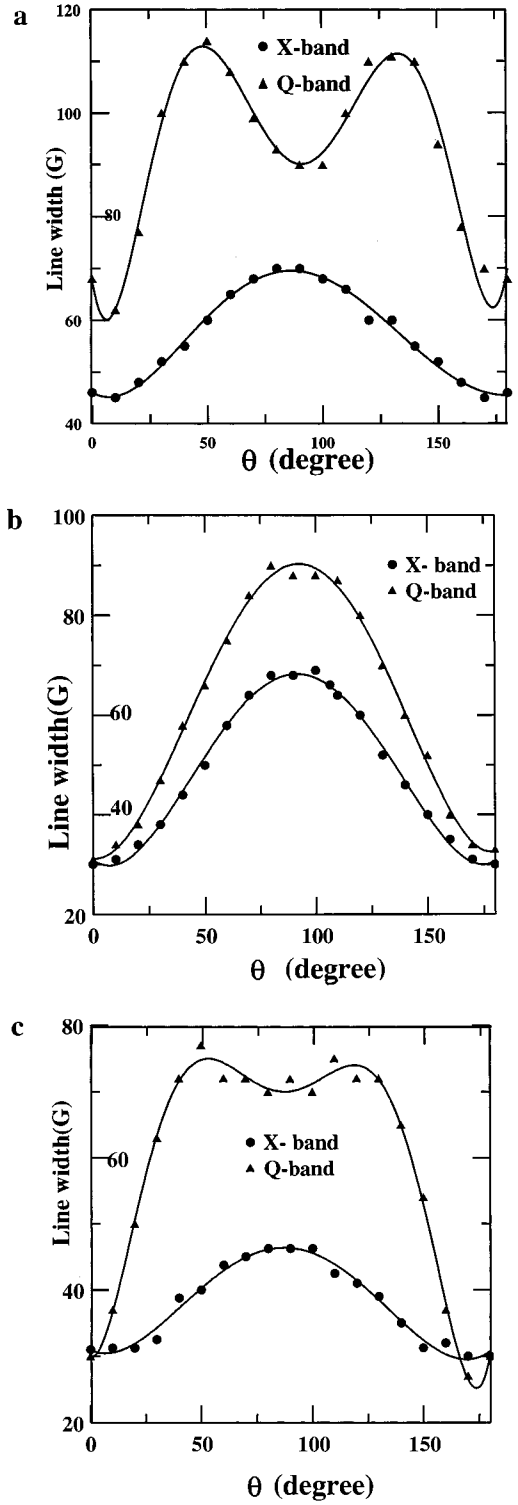


**Figure 9.** Angular variations of line widths in the (a) *bc*, (b) *ac*, and (c) *ab* planes for $[Cu(dpt)(en)](ClO_4)_2$.

different sites) at Q-band, as well. Therefore

$$A(\text{hyperfine}), D(\text{dipolar}) < (\Delta g)\beta B_0$$

$$(\text{between the sites at X- and Q-bands}) < J$$

**(b) Interstack Exchange, *J′*.** The line width variations at X- and Q-band frequencies in the *ac* plane were used to estimate the effective intersite exchange field, $H_e$, as well as $J'$. For $J' > (\Delta g)\beta B/2$, we would observe a single line and the theories of exchange averaging predict that the width varies as the square of the splitting $\Delta B$ (in gauss) between the sites[22]

$$\Delta B_{pp} = (\Delta B)^2/H_e \tag{4}$$

where $H_e$ is defined as the effective intersite exchange field. If the measurements are performed at two different frequencies, e.g, X- and Q- band, then

$$\Delta B_{pp}{}^{Q} - \Delta B_{pp}{}^{X} = [(\Delta B_Q)^2 - (\Delta B_X)^2]/H_e \tag{5}$$

where $\Delta B_X$ and $\Delta B_Q$ are the differences in the expected resonance fields of the two sites at X- and Q-band, respectively, in the absence of $J'$. The quantity $H_e$ depends on the rate of exchange between inequivalent sites and is given by[23]

$$(g\beta/\eta)H_e = 4t_c{}^{-1}(3^{1/2}/2) \tag{6}$$

where $t_c = 0.16\ \mathrm{h}|J|^{1/3}/J'|^{4/3}$ is the correlation time for interchain spin diffusion. The calculated $H_e$ of 158 G from the *ac* plane gives a value of $1.2 \times 10^{-9}$ s for $t_c$. The line width variation does not follow a $|3\cos^2\theta - 1|^{4/3}$ dependence.

**(c) Intrastack Exchange, *J*.** The intrastack exchange parameter $J$ can be estimated from the line width variation in the *bc* plane. In this plane, the two sites are equivalent and the effective field is given by[22]

$$\mathbf{B}_e = \mathbf{B}\cdot\Delta g$$

The effective field $\mathbf{B}_e$ is seen perpendicular to the *bc* plane, where the axis of quantization defined by $\mathbf{B}\cdot\mathbf{g}$ lies, and will give rise to nonsecular broadening effects. The above effect is shown to be negligible when $\omega_0 t_c \gg 1$.[24] In our case, $t_c = 1.2 \times 10^{-9}$ s (vide supra) and hence $\omega_0 t_c = 11$ at X-band and 42 at Q-band. Therefore, the nonsecular contribution to the line width can be neglected. In the strong-exchange-narrowing case, the line width $\Delta B_{pp}$ is given by[25]

$$(3^{1/2}/2)\Delta B_{pp} = M_2{}^{t}/J \tag{7}$$

where $M_2{}^t$ is the sum of dipolar and hyperfine second moments and $\Delta B_{pp}$ is the local field. The full second moment is used when $J \gg \eta\omega_0$, where $\omega_0$ is the Zeeman frequency. When $J \ll \omega_0$, only the secular ($\Delta m = 0$) part of the second moment will be effective in contributing to the observed line width[26]

$$M_2{}^{t} = M_2{}^{0} + a^0$$

where $M_2{}^0$ is the secular part of the dipolar second moment and $a^0$ is the secular part of the hyperfine second moment. The secular contribution of the dipolar second moment for $S = {}^1/_2$ is[26,27]

$$M_2{}^{0} = \frac{9}{16} g^4\beta^4 \sum_{i\neq j} (3\cos^2\psi_{ij} - 1)^2 r_{ij}{}^{-6} \tag{8}$$

where $\cos\psi_{ij} = [g_{||}/g(\theta)]\cos\theta_{ij}$; $g^2 = (g_1{}^2 + g_2{}^2 + g_3{}^2)/3$; $r_{ij}$ is the distance between the two spin centers; $\psi_{ij}$ is the angle between $r_{ij}$ and the effective field $gB_0$; $\beta$ is the Bohr magneton;

(22) Yokota, M.; Koide, S. *J. Phys. Soc. Jpn.* **1954**, *9*, 953.
(23) Hughes, R. C.; Morosin, B.; Richards, P. M. *Phys. Rev. B* **1975**, *11*, 1795.
(24) Ramakrishna, B. L.; Manoharan, P. T. *Mol. Phys.* **1984**, *52*, 65.
(25) van Vleck, J. H. *Phys. Rev.* **1948**, *73*, 1248.
(26) McGregor, K. T.; Soos, Z. G. *J. Chem. Phys.* **1976**, *64*, 2506.
(27) Soos, Z. G.; Huang, T. Z.; Valentine, J.; Hughes, R. C. *Phys. Rev. B* **1973**, *8*, 993.

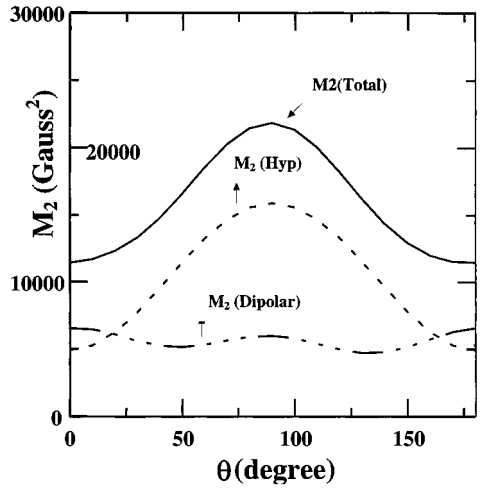


**Figure 10.** Angular variations of local fields in the *bc* plane for [Cu(dpt)(en)]$(ClO_4)_2$.

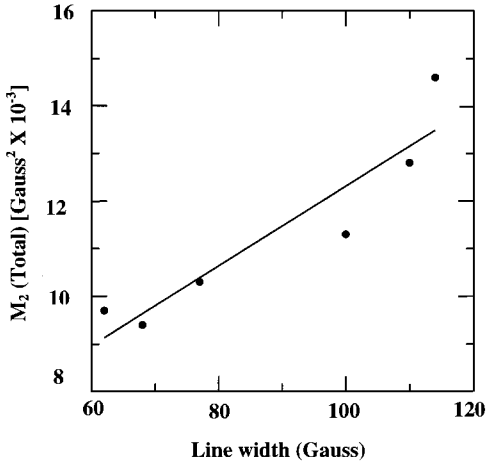


**Figure 11.** Correspondence between the local fields and line widths in the *bc* plane for [Cu(dpt)(en)]$(ClO_4)_2$. The continuous line corresponds to calculated line widths and, the filled circles are the measured line widths.

and $\theta_{ij}$ is the angle between $r_{ij}$ and $B_0$. The secular contribution of the hyperfine second moment is given by

$$\eta^2 a^0 = {}^1/_3 I(I+1)K^2 \qquad (9)$$

where $I$ is the nuclear spin (Cu, $I = {}^3/_2$); $g^2(\theta) = g_1^2 \cos^2\theta_1 + g_2^2 \cos^2\theta_2 + g_3^2 \cos^2\theta_3$; and $K^2g^2(\theta) = (A_1^2g_1^2 \cos^2\theta_1 + A_2^2g_2^2 \cos^2\theta_2 + A_3^2g_3^2 \cos^2\theta_3)$. The angular variation of the total second moment is shown in Figure 10. Here the second moment due to the hyperfine part is greater than that due to the dipolar part, since all the nearest Cu- - -Cu distances are greater than 7 Å.

Though the data at one orientation are sufficient to estimate $J$ using eq 7, we find from Figure 11 that there is good agreement between the two quantities over the entire set of data in this plane. The fitting gives a value of 280 G for $J$ for the room-temperature data in the *bc* plane. The $J'$ value calculated with the aid of $t_c$ and $J$ is 18 G. The very small $J'/J$ ratio of $6 \times 10^{-2}$ is low enough to make the interaction one-dimensional but at the same time sufficient enough to cut off the long-time diffusive behavior of spins in pure 1-D chains giving rise to the observed Lorentzian line shapes. In some of the orientations, the magnitude of interaction is comparable to the hyperfine coupling constant, where the peaks tend to resolve. The

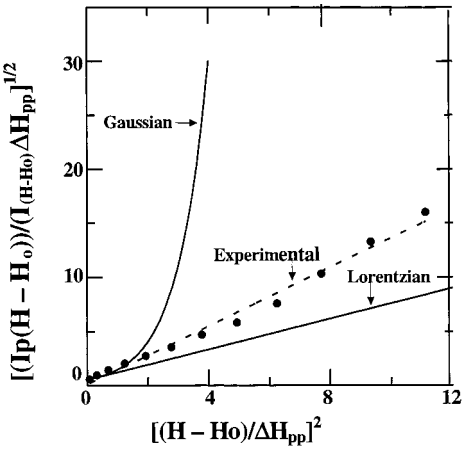


**Figure 12.** EPR line shape analysis for an arbitrary orientation in the *bc* plane for [Cu(dpt)(en)]$(ClO_4)_2$. The dashed line is a guide for the eye.

magnitude of $\Delta g$ between the two different sites is very small in all orientations, leading to a single magnetically distinct site at both X- and Q-band frequencies.

In the system $[Cu_2(Me_5dien)_2(C_2O_4)](ClO_4)_2$ when the perchlorate anion is replaced by the tetraphenylborate anion, the exchange interaction is greatly attenuated and the hyperfine lines become resolved in the EPR spectrum of the neat polycrystalline sample.[10] The tetraphenylborate anion keeps the interacting centers well separated; the exchange interactions are reduced, and the anion is not involved in the exchange mechanism. This is indirect evidence for the perchlorate anion being involved in the exchange interaction pathway. The same mechanism is operative in the present complex also.

When the perchlorate anion is replaced by the tetraphenylborate anion, exchange is arrested.[17] It is therefore concluded that the perchlorate anion mediates the superexchange pathway.

**(d) Line Shapes.** Line shape analysis was carried out for the spectrum for an arbitrary orientation in the *bc* plane. This is depicted in the Figure 12. The experimental line shape function is Lorentzian in nature with a slight deviation toward a Gaussian function and is presumably due to the weak interchain exchange. This line shape analysis confirms the behavior of the system as quasi-one-dimensional, and as expected it falls between Lorentzian and Gaussian functions and closer to the FT of $\exp(-t^{3/2})$.

## Conclusions

Single-crystal XRD shows that the molecular structure of the title complex is distorted trigonal bipyramidal. EPR studies reveal that the ground state of the molecule is formally $d_{z^2}$. The ratio of interstack/intrastack exchange and correlation time for spin diffusion ($t_c$) show that the system behaves as a quasi-one-dimensional magnetic material. The magnitude of the intrastack exchange coupling constant is of the order of maximum copper hyperfine coupling but is less than the $g$ anisotropy at both X- and Q-band frequencies. This leads to the expected absence of any hyperfine splitting at both frequencies. Whereas, normally, the $g$ anisotropy would have led to the resolution of magnetically distinct sites, this has not happened for the simple reason that at any orientation the $\Delta g$ between the two sites is always less than $J$. The availability of the isomorphous zinc lattice has helped in obtaining reliable values of magnetic parameters for the isolated molecule. The reintroduction of resolved copper hyperfine coupling when the perchlorate anion is replaced by the tetraphenylborate anion is indirect, nevertheless conclusive, evidence that the former must

be involved in the superexchange pathway and the observed weak quasi-one-dimensional magnetic behavior. This is further confirmed by the nature of the line shape.

**Supporting Information Available:** Listings of structure refinement details, atomic positional and thermal parameters, anisotropic thermal parameters, and full bond distances and bond angles (6 pages). Ordering information is given on any current masthead page.

IC980071N